A. Kuzmin, J. Timoshenko, A. Kalinko, I. Jonane, A. Anspoks,
Treatment of disorder effects in X-ray absorption spectra beyond the conventional approach,
Rad. Phys. Chem. 175 (2020) 108112.

Treatment of disorder effects in X-ray absorption spectra beyond the conventional approach

Alexei Kuzmin[a,b,*], Janis Timoshenko[c], Aleksandr Kalinko[d], Inga Jonane[a], Andris Anspoks[a]

[a] *Institute of Solid State Physics, University of Latvia, Kengaraga street 8, LV-1063 Riga, Latvia*
[b] *International Research Organization for Advanced Science and Technology (IROAST), Kumamoto University, 2-39-1 Kurokami, Chuo-ku, Kumamoto 860-8555, Japan*
[c] *Department of Materials Science and Chemical Engineering, Stony Brook University, Stony Brook, NY 11794, USA*
[d] *Universität Paderborn, Naturwissenschaftliche Fakultät, Department Chemie, Warburger Strasse 100, 33098 Paderborn, Germany*

Abstract

The contribution of static and thermal disorder is one of the largest challenges for the accurate determination of the atomic structure from the extended X-ray absorption fine structure (EXAFS). Although there are a number of generally accepted approaches to solve this problem, which are widely used in the EXAFS data analysis, they often provide less accurate results when applied to outer coordination shells around the absorbing atom. In this case, the advanced techniques based on the molecular dynamics and reverse Monte Carlo simulations are known to be more appropriate: their strengths and weaknesses are reviewed here.

Keywords: X-ray absorption spectrocopy, Extended X-ray absorption fine structure (EXAFS), Molecular dynamics, Reverse Monte Carlo, Static and thermal disorder

1. Introduction

X-ray absorption spectroscopy (XAS) is an excellent tool to probe the local environment in crystalline, nanocrystalline and disordered solids, liquids and gases in a wide range of *in situ* and *in operando* conditions (van Oversteeg et al. (2017); Mino

*Corresponding author
Email address: a.kuzmin@cfi.lu.lv (Alexei Kuzmin)
URL: http://www.cfi.lu.lv (Alexei Kuzmin)

et al. (2018)). With the increased availability of synchrotron radiation sources and the tremendous improvement in their parameters, the popularity of the technique has increased, and the quality of the experimental X-ray absorption spectra has improved significantly. As a result, more accurate and reliable structural information can be extracted from the extended X-ray absorption fine structure (EXAFS) located above the absorption edge of an element.

The quantitative analysis of EXAFS became possible due to significant advancements in the theory (Rehr and Albers (2000); Natoli et al. (2003); Rehr et al. (2009)), however, accurate treatment of disorder effects is still the biggest difficulty. The problem becomes especially acute when it comes to the outer coordination shells around the absorbing atom, where the overlap of the shells and the effect of the disorder are mixed with the multiple-scattering (MS) contributions.

This paper reviews the existing approaches commonly used to solve the problem of disorder in EXAFS and discusses the strengths and weaknesses of two advanced techniques based on the molecular dynamics and reverse Monte Carlo methods.

2. Conventional approach to disorder in EXAFS

In this section, we will briefly summarize different conventional approaches to the treatment of disorder in EXAFS.

The X-ray absorption coefficient $\mu(E)$ in the one-electron approximation is proportional to the transition rate between the initial core-state i and the final excited-state f of an electron, which is given by the Fermi's Golden rule

$$\mu(E) \propto \sum_f \left|\langle f|\hat{H}|i\rangle\right|^2 \delta(E_f - E_i - E) \tag{1}$$

where $E = \hbar\omega$ is the X-ray photon energy, and the transition operator $\hat{H} = \hat{\epsilon} \cdot \vec{r}$ in the dipole approximation. Note that the final state of the electron is the relaxed excited state in the presence of the core-hole screened by other electrons.

The characteristic time of the photoabsorption process (1) is about 10^{-15}–10^{-16} s and is determined by several processes: the transition time between initial (i) and final (f) states, the core-hole lifetime, the excited photoelectron relaxation time and the lifetime of the photoelectron out of atom related to its mean-free path (MFP). Note that this time is significantly shorter than the characteristic time ($\sim 10^{-13}$–10^{-14} s) of thermal vibrations. Therefore, atoms can be considered as frozen at their instantaneous positions during the excitation process, and the experimental X-ray absorption spectrum corresponds to the average over all atomic configurations during the time of experiment.

The oscillating part of the absorption coefficient $\chi^l(E)$ located above the absorption edge of orbital type l is defined as

$$\chi^l(k) = (\mu(E) - \mu_0(E) - \mu_b(E))/\mu_0(E)) \tag{2}$$

where $\mu_b(E)$ is the background absorption, and $\mu_0(E)$ is the atomic-like absorption due to an isolated absorbing atom (Lee et al. (1981)). The wave number k of the excited photoelectron is related to its kinetic energy $(E - E_0)$ by $k = \sqrt{(2m_e/\hbar^2)(E - E_0)}$, where m_e is the electron mass, $\hbar$ is the Plank's constant, and E_0 is the threshold energy, i.e., the energy of a free electron with zero momentum.

Within the framework of MS theory, EXAFS $\chi^l(k)$ is described using a series

$$\begin{aligned} \chi^l(k) &= \sum_{n=2}^{\infty} \chi^l_n(k), \\ \chi^l_n(k) &= \sum_j A^l_n(k, R_j) \sin[2kR_j + \phi^l_n(k, R_j)] \end{aligned} \tag{3}$$

which includes contributions $\chi^l_n(k)$ from the $(n-1)$-order scattering processes of the excited photoelectron by the neighbouring atoms, before it returns to the absorbing atom (Ruiz-Lopez et al. (1988); Rehr and Albers (2000)). The fast convergence of the MS series occurs at least at high-k values due to the finite lifetime of the excitation, the scattering path lengths, interference cancellation effects and path disorder. In practice, the MS contributions up to the 8th-order can be calculated using *ab initio* FEFF code (Ankudinov et al. (1998); Rehr et al. (2010)).

An alternative description of the EXAFS $\chi^l(k)$ in terms of the n-order distribution functions $g_n(R)$ is also known

$$\chi^l(k) = \int 4\pi R^2 \rho_0 g_2(R) [\chi_2^{oio}(k) + + \ldots] dR$$

$$
\begin{aligned}
&+ \iiint 8\pi^2 R_1^2 R_2^2 \sin(\theta)\rho_0^2 g_3(R_1, R_2, \theta) \\
&\times [2\chi_3^{oijo}(k) + 2\chi_4^{oiojo}(k) + \ldots] dR_1 dR_2 d\theta \\
&+ \ldots \qquad (4)
\end{aligned}
$$

where ρ_0 is the average density of a system and $\chi_m(k)$ are the MS EXAFS signals of the $(m-1)$ order generated within a group of atoms (o, i, j, ...) described by g_n (Filipponi et al. (1995); Filipponi and Di Cicco (1995)). This approach was realized in the GNXAS code (Di Cicco (1995); Filipponi and Di Cicco (2000)), which is able to account for the two-body (g_2), three-body (g_3) and four-body (g_4) distribution functions.

The analytical expression for EXAFS can be greatly simplified when one needs to extract information only on the first coordination shell of the absorbing atom.

The contribution of the first coordination shell to the total EXAFS spectrum can be usually isolated by Fourier filtering procedure and analysed within the single-scattering approximation, since the length of all MS paths is longer than the first coordination shell radius. Thus, only the first term of the series given by Eq. (3) remains. In the case of a Gaussian distribution (or in the harmonic approximation), the EXAFS expression takes a simple form

$$
\begin{aligned}
\chi_2^l(k) &= S_0^2 \sum_i N_i \frac{|f_{\text{eff}}^l(k, R_i)|}{kR_i^2} \exp\left[-\frac{2R_i}{\lambda(k)}\right] \\
&\times \sin[2kR_i + \phi^l(k, R_i)] \exp(-2\sigma_i^2 k^2) \qquad (5)
\end{aligned}
$$

where S_0^2 is a scaling factor; N_i is the coordination number; R_i is the interatomic distance; $\lambda(k)$ is the photoelectron MFP; $f_{\text{eff}}^l(k, R)$ and $\phi^l(k, R)$ are the photoelectron effective scattering amplitude and phase shift functions (Sayers et al. (1971); Lee and Pendry (1975)). The sum in Eq. (5) is taken over groups of atoms located at different distances from the absorber.

For moderate disorder, when distribution of interatomic distances becomes asymmetric, the EXAFS equation can be expressed using the cumulant decomposition (Bunker (1983); Dalba et al. (1993)). The cumulant model is often useful for the analysis of anharmonic and thermal expansion effects (Tranquada and Ingalls (1983); Fornasini et al. (2017)), nanoparticles (Clausen and Nørskov (2000); Sun et al. (2017)) and disordered materials (Dalba et al. (1995); Okamoto et al. (2002)).

Sometimes, the first coordination shell around the photoabsorber is so strongly distorted that the cumulant series does not converge. In this case, the EXAFS formula expressed in terms of the radial distribution function (RDF) $G(R)$

$$\begin{aligned}\chi_2^l(k) &= S_0^2 \int_{R_{\min}}^{R_{\max}} G(R) \frac{|f_{\rm eff}^l(k,R)|}{kR^2} \\ &\times \sin[2kR + \phi^l(k,R_i)] \exp\left[-\frac{2R_i}{\lambda(k)}\right] dR \end{aligned} \tag{6}$$

should be used instead (Stern et al. (1975); Lee et al. (1981)). The RDF $G(R)$ defines the probability of finding an atom in a spherical shell dR at the distance R from the photoabsorber. The number N of atoms located in the range between $R_{\min}$ and $R_{\max}$ is given by the integral $N = \int_{R_{\min}}^{R_{\max}} G(R)dR$. To determine RDF $G(R)$ from Eq. (6), the regularization technique (Babanov et al. (1981); Ershov et al. (1981); Kuzmin and Purans (2000)) can be used to solve this integral equation as an ill-posed problem without any preliminary assumption on the shape of the RDF. This approach was recently used to reconstruct the local structure in several tungstates MWO_4 (M=Ni, Cu, Zn and Sn) (Kalinko and Kuzmin (2011); Anspoks et al. (2014); Kuzmin et al. (2015)) and in molybdate $CuMoO_4$ (Jonane et al. (2018b)), where the Jahn-Teller effect is responsible for a strong distortion of structural units. It was demonstrated recently that the RDF $G(R)$ of atoms can be reliably extracted up to distant coordination shells using neural network approach (Timoshenko et al. (2018)).

In crystalline and nanocrystalline materials, the experimental EXAFS spectrum often contains a significant amount of structural information on outer coordination shells, which is challenging to extract. It is possible to estimate the region of a structure around the absorber, which can potentially contribute into EXAFS, from the photoelectron MFP. Examples for bulk and nanocrystalline nickel oxide (Anspoks et al. (2012)) and body-centred-cubic (bcc) tungsten (Jonane et al. (2018a)) are shown in Fig. 1. A half of the MFP $\lambda(k)$ gives an estimate of how far the excited photoelectron can propagate to be able to return back to the absorbing atom. The MFP $\lambda(k)$ depends strongly on the photoelectron wavenumber k and increases at large k-values. It is equal to about 10–20 Å for NiO or bcc W at $k \approx$ 16–20 Å^{-1}. This means that when high-quality experimental EXAFS data are available in large k-space range, one can expect to see structural contributions from atoms located in distant coordination shells. For example, the structural peaks in Fourier transforms of EXAFS can be recognized up to about 11 Å in Fig. 1 for bulk and nanosized NiO at $T = 10$ K and for bcc W at $T = 300$ K.

The possibility to analyse contributions from distant coordination shells is useful since it provides access to additional structural information. However, such analysis based on the conventional approaches faces a number of problems even for crystalline materials with a known structure, in which at least the mean-square relative displacement (MSRD) factors are variable model parameters.

The main problem is related to the number of model parameters, which increases exponentially when more coordination shells are included to the model (Kuzmin and Chaboy (2014)). For example, in the case of bulk NiO with a rock-salt structure, the total number of scattering paths, the number of unique paths due to the cubic symmetry and the maximum number of fitting parameters, which can be used in the EXAFS model according to the Nyquist criterion ($N_{\rm par} = 2\Delta k \Delta R/\pi$) evaluated for relatively long EXAFS signal with Δk=20 Å^{-1}, are shown in Fig. 2 as a function of the cluster radius R around the photoabsorbing nickel atom. Note that the Nyquist criterion is not satisfied above R~5.5 Å, when cubic crystal symmetry is taken into account, but this distance decreases significantly down to R~3.5 Å in a nanomaterial.

To reduce the number of model parameters, one can evaluate the MSRD factors semiempirically from correlated Einstein or Debye models (Sevillano et al. (1979); Vaccari and Fornasini (2006)), but again different Einstein or Debye temperatures are required for each MS path. Besides, these models of lattice dynamics ignore anisotropy of the phonon spectra.

Another approach is to calculate MSRD parameters from the phonon projected density of states using the Debye integral

$$\sigma_R^2(T) = \frac{\hbar}{2\mu_R} \int_0^\infty \frac{1}{\omega} \coth\left(\frac{\hbar\omega}{2k_B T}\right) \rho_R(\omega) d\omega \qquad (7)$$

where μ is the reduced mass associated with the MS path, and k_B is the Boltzmann's constant. The vibrational density of states $\rho_R(\omega)$ projected on R can be obtained from first-principles calculations of the dynamical matrix of force constants (Vila et al. (2007); Rehr et al. (2009, 2010)). However, this approach uses (quasi-)harmonic approximation, requires *a priori* knowledge of structure and can be computationally expensive.

An alternative solution which allows one to account simultaneously for the MS contributions and disorder effects is to rely on atomistic simulations such as the molecular dynamics (MD) and reverse Monte-Carlo (RMC) methods combined with ab initio MS calculations.

3. Atomistic simulations of EXAFS

MD (Alder and Wainwright (1957)) and RMC (McGreevy and Pusztai (1988)) methods are known for a long time, however their application in the field of X-ray absorption spectroscopy is still scarce. The use of both methods requires significant computing resources, so their development has been directly related to the advances in computer technologies.

The first use of MD simulations to reproduce the experimental EXAFS is dated back to the middle of nineties, when the method was applied to study the hydration of ions in aqueous solutions (D'Angelo et al. (1994, 1996); Palmer et al. (1996); Kuzmin et al. (1997)). The advantages of the RMC method were realized even earlier at the beginning of nineties, when it was used to interpret EXAFS of amorphous Si and crystalline AgBr (Gurman and McGreevy (1990)), liquid KPb alloys (Bras et al. (1994)) and superionic glasses (Wicks et al. (1995)).

There are several common features for the MD and RMC methods. The simulation result is represented as one or more atomic configurations ("snapshots"), suitable to generate the configuration-averaged (CA) EXAFS, which includes static and dynamic disorder and can be directly compared to experimentally measured EXAFS. The static disorder is due to a number of different atomic dispositions, corresponding to minima of the potential energy surface. Examples of systems with the static disorder include non-crystalline materials such as glasses, amorphous solids and liquids, nanocrystals and thin films with atomic structure relaxed due to the size or thickness reduction effect, and materials with structural defects (e.g., vacancies or grain boundaries). Dynamic disorder arises from temperature-dependent fluctuations in the atomic positions from the equilibrium structure.

The CA EXAFS spectra for different absorption edges can be calculated from the same set of atomic coordinates and used in the analysis, thus improving the reliability of the structural model (Timoshenko et al. (2014a)). During a simulation, the atoms are placed in a cell of the required size and shape, often with periodic boundary conditions (PBC) in order to avoid effects associated with the surface. Note that using PBC limits the maximum cluster radius, for which EXAFS calculations can be safely performed to avoid artificial correlation effects, to half the minimum cell size. There are also two non-structural parameters, ΔE_0 and S_0^2, which are required for comparison with the experimental EXAFS. They can be determined from the analysis of reference materials or obtained by best matching the experimental and calculated EXAFS spectra.

The scheme of the MD and RMC methods is shown in Fig. 3. The structural model of a material is constructed first in both cases, and the *ab initio* MS code, such as FEFF (Ankudinov et al. (1998)) or GNXAS (Filipponi and Di Cicco (2000)), is used to calculate EXAFS for each atomic configuration during the simulation.

The principal difference between two methods is that no fitting of experimental EXAFS is performed in the MD-EXAFS approach, and the structure obtained in the MD simulation is used “as-is” for the calculation of the CA EXAFS. Note that the number of required atomic configurations and the time step between them should be carefully estimated for each particular case to obtain the proper CA signal. On the contrary, the structural model is modified at each RMC iteration to minimize the difference between the experimental and CA EXAFS in the RMC-EXAFS approach.

To perform MD simulations, a model of interactions between atoms is required. In classical MD (CMD), the empirical interatomic potential is employed, that significantly reduces the requirements for computing resources. Besides, the MD-EXAFS approach is suitable for a validation of interatomic potential along with other conventionally employed properties of a material (Di Cicco et al. (2002); Kuzmin and Evarestov (2009); Kuzmin et al. (2016); Bocharov et al. (2017)). *Ab initio* MD (AIMD) based on density functional theory (DFT) formalism is also accessible nowadays but is extremely computationally expensive. It is important that in the MD simulation, initial model of the atomic structure is evolving in time within one of the canonical (NVT), isothermal–isobaric (NpT) or microcanonical (NVE) ensembles following to classical Newtonian laws of motion both in CMD and AIMD. Therefore, such simulations cannot be used to model the motion of atoms at low temperatures, where the zero-point oscillations of atoms play an important role (Yang and Kawazoe (2012)). In this case, instead, more complex methods should be used, such as, for example, the path-integral MD (Marx and Parrinello (1996)).

Note that recent developments of X-ray free-electron laser (X-FEL) facilities open new possibilities to probe the ultrafast excited state dynamics using X-ray absorption spectroscopy (Lemke et al. (2017)). Such experiments provide information on the femtosecond nuclear wavepacket dynamics, which can be described by first-principles quantum dynamics simulations (Capano et al. (2015)).

The MD simulations can be performed, for example, either by one of the CMD codes as LAMMPS (Plimpton (1995)), GULP (Gale and Rohl (2003)) or DL_POLY (Todorov et al. (2006)), or using AIMD codes as CP2K (VandeVondele et al. (2005)), VASP (Kresse and Furthmüller (1996)) or SIESTA (Soler et al. (2002)). After accumulating the required number of atomic configurations, one can employ, for example, the EDACA code (Kuzmin and Evarestov (2009); Kuzmin et al. (2016)) to generate the CA EXAFS spectrum.

In RMC simulation, the position of atoms in the configuration is usually randomly modified at each iteration, and the CA EXAFS signal is calculated. The decision to accept or reject the new atomic configuration is made based on the Metropolis algorithm (Metropolis et al. (1953)), taking into account the difference (residual) between the experimental and simulated data in either k or R space, or simultaneously in k and R-spaces using the wavelet transformation (Timoshenko and Kuzmin (2009)). At this point, various chemical or geometrical constraints can be easily implemented, by assigning some penalty to the residual value. For example, one can avoid situations when the atoms are getting too close or too far from each other, when non-physical values of some bond angle are found (Tucker et al. (2007)), or when the coordination number for some atom deviates from the expected one (McGreevy (2001)), etc. The efficiency of the RMC process can be significantly improved by using an evolutionary algorithm (EA) together with a simulated annealing scheme (Timoshenko et al. (2012, 2014b)).

The RMC method relies on stochastic process, so it will generate different final sets of atomic coordinates upon restarting simulation several times from different starting conditions. However, it is expected that the results will be statistically close in terms of the distribution functions. Note that RMC method tends to converge to the most disordered solution consistent with the experimental data (Tucker et al. (2007)).

Some of the software packages for RMC-EXAFS simulations include RMC-GNXAS (Di Cicco and Trapananti (2005)), RMCProfile (Tucker et al. (2007)), EPSR-RMC (Bowron (2008)), SpecSwap-RMC (Leetmaa et al. (2010)), RMC++/RMC_POT (Gereben et al. (2007); Gereben and Pusztai (2012)) and EvAX (Timoshenko et al. (2014b)).

Note that in addition to the MD and RMC methods, the average atomic configuration required to compute CA EXAFS can also be generated from a Monte Carlo simulation based on interatomic potentials (Hansen et al. (1997); Canche-Tello et al. (2014); House et al. (2017)) or atomic displacement parameters obtained from lattice dynamics calculations (Duan et al. (2016); Lapp et al. (2018)).

4. Examples of MD/RMC-EXAFS applications

In this section the specific capabilities of the MD-EXAFS and RMC-EXAFS methods will be demonstrated.

The first example is concerned with the lattice dynamics in bcc tungsten (Jonane et al. (2018a)). High-quality experimental W L_3-edge EXAFS spectrum was recorded at $T = 300$ K up to $k = 18$ Å^{-1} (Fig. 4 (upper panel)) and includes contributions from the coordination shells with a radius of at least up to ∼11 Å (Fig. 1 (lower panel)). The NVT MD simulations were performed by the GULP code (Gale and Rohl (2003)) using a supercell of $7a_0 \times 7a_0 \times 7a_0$ size ($a_0 = 3.165$ Å) and a time step of 0.5 fs. The interactions were described by the second nearest-neighbour modified embedded atom method (2NN-MEAM) potential (Lee et al. (2001)). After equilibration during 20 ps, the atomic configurations were accumulated during the production run of 20 ps and used to calculate the CA EXAFS. The RMC/EA calculations were performed by the EvAX code (Timoshenko et al. (2014b)) using a supercell of $5a_0 \times 5a_0 \times 5a_0$ size to get best possible agreement between the Morlet wavelet transforms (WTs) of the experimental and calculated EXAFS spectra. Good agreement with the experimental EXAFS data was obtained for both MD-EXAFS and RMC-EXAFS approaches (Fig. 4 (upper panel)). Next, the atomic configurations were used to calculate the RDFs $G_{\mathrm{W-W}}(R)$ and the radial dependence of the MSRD factors $\sigma^2(R)$. At long distances, when correlation in atomic motion becomes negligible, the MSRD $\sigma^2_{\mathrm{W-W}} = 2\sigma^2_{\mathrm{W}}$ (see the inset in Fig. 4 (lower panel)). The obtained mean square displacements (MSD) σ^2_{W} are in agreement with previously reported experimental and theoretical results (Jonane et al. (2018a)). Thus, the analysis of distant coordination shells allows extracting information on the MSD of atoms, which otherwise requires a diffraction experiment.

In the second example, the use of the MD-EXAFS approach for the validation of the interatomic potential model is shown on the example of iron fluoride (FeF_3) (Jonane et al. (2016)). The crystalline lattice of rhombohedral FeF_3 is composed of FeF_6 octahedra joined by corners with the bond angle Fe–F–Fe between two adjacent octahedra equal to ~153°. The MD simulations were carried out using a simple empirical potential, including two-body (Fe–F and F–F) and three-body (Fe–F–Fe) interactions. It was found that different sets of the optimized potential parameters, corresponding to the iron effective charge q(Fe) in the range of 1.2–3.0, reproduce equally well the static crystallographic structure of FeF_3. This ambiguity was resolved by performing NVT CMD simulations and calculating the CA Fe K-edge EXAFS spectra (Fig. 5). Strong sensitivity of EXAFS to the strength of the Coulomb interactions was found, thus allowing one to select the iron effective charge q(Fe)=1.71 giving the best overall agreement between the experimental and CA EXAFS spectra.

Final example demonstrates the possibility to probe anisotropy and correlation of atomic motion in copper nitride (Cu_3N) using the RMC-EXAFS approach (Fig. 6) (Timoshenko et al. (2017)). Cu_3N has a unique cubic anti-perovskite-type structure (AB_3X), composed of NCu_6 octahedra joined by the corners with the A sites being vacant. High symmetry of its lattice is responsible for strong overlap of coordination shells in the RDF, large MS contributions in EXAFS due to the presence of linear –Cu–N–Cu– chains and an anisotropy of atom vibrations due to tilting motion of NCu_6 octahedra. Since RMC simulation results in a 3D model of the structure, one has an opportunity to analyse separately behaviour of atoms, belonging to different coordination shells but located at close distances from the absorber. Temperature dependences of the MSRD factors for selected Cu–N and Cu–Cu atom pairs were calculated from atomic configurations obtained by RMC and are shown in Fig. 6 (lower panel). Strong correlation in atomic motion was found for atoms (N_1, Cu_{3a} and N_{7a}) located in the chains along the crystallographic axes. Moreover, it is possible to distinguish clearly large difference in the MSRD factors of non-equivalent atoms located in the 3rd (Cu_{3a} and Cu_{3b}) and 7th (N_{7a} and N_{7b}) shells. Strong increase of the MSRD of Cu_{3a}, Cu_2 and Cu_{3b} points to the anisotropic vibration of copper atoms in the direction orthogonal to –N–Cu–N– chains.

5. Conclusions

Atomistic simulation methods such as molecular dynamics and reverse Monte Carlo provide a natural way to include disorder (static and dynamic) into the EXAFS formalism taking into account multiple-scattering effects.

The two methods have several common points. In both cases, multiple absorption edges can be easily simulated or fitted, thus improving the reliability of the accessible structural information. The analysis of EXAFS contributions from outer coordination shells of the absorbing atom is feasible, which is rather challenging in conventional approach but provides an access to some useful structural and dynamic properties of a material as, for example, mean-square displacements.

Opposite to conventional analysis, dealing with a set of structural parameters, MD-EXAFS and RMC-EXAFS approaches provide a result in terms of atomic configurations, giving information on atom-atom and bond-angle distributions and correlations. Moreover, an access to atomic coordinates makes it possible to distinguish contributions of non-equivalent atom pairs with equal or close path lengths.

At the same time, there are also several differences between the two methods.

The MD-EXAFS approach does not require any structural fitting parameters, and the structural model of a material is uniquely defined by the results of the MD simulation. The agreement between the experimental and calculated CA EXAFS spectra depends on the accuracy of interatomic potential model, therefore, EXAFS spectrum can be used to validate the interatomic potentials.

3D structure models obtained by the RMC method from experimental EXAFS can be directly compared with the results of other atomistic simulations. Moreover, they can be employed to include disorder effects into first-principles simulations to predict temperature dependent material properties. Note that constraints can be easily incorporated into the RMC analysis to account for information from other experiments (diffraction, total scattering, etc) or chemical/geometrical information (bond-lengths, bonding angles, coordination, energetics, etc).

Acknowledgements

This work has been partially supported by the Latvian Council of Science project no. lzp-2018/2-0353.

References

Alder, B.J., Wainwright, T.E., 1957. Phase transition for a hard sphere system. J. Chem. Phys. 27, 1208–1209. doi:10.1063/1.1743957.

Ankudinov, A.L., Ravel, B., Rehr, J.J., Conradson, S.D., 1998. Real-space multiple-scattering calculation and interpretation of X-ray-absorption near-edge structure. Phys. Rev. B 58, 7565–7576. doi:10.1103/PhysRevB.58.7565.

Anspoks, A., Kalinko, A., Kalendarev, R., Kuzmin, A., 2012. Atomic structure relaxation in nanocrystalline NiO studied by EXAFS spectroscopy: Role of nickel vacancies. Phys. Rev. B 86, 174114. doi:10.1103/PhysRevB.86.174114.

Anspoks, A., Kalinko, A., Timoshenko, J., Kuzmin, A., 2014. Local structure relaxation in nanosized tungstates. Solid State Commun. 183, 22–26. doi:10.1016/j.ssc.2013.12.028.

Babanov, Y.A., Vasin, V.V., Ageev, A.L., Ershov, N.V., 1981. A new interpretation of EXAFS spectra in real space. I. General formalism. Phys. Status Solidi B 105, 747–754. doi:10.1002/pssb.2221050237.

Bocharov, D., Chollet, M., Krack, M., Bertsch, J., Grolimund, D., Martin, M., Kuzmin, A., Purans, J., Kotomin, E., 2017. Analysis of the U L_3-edge X-ray absorption spectra in UO_2 using molecular dynamics simulations. Prog. Nucl. Energy 94, 187–193. doi:10.1016/j.pnucene.2016.07.017.

Bowron, D.T., 2008. Experimentally consistent atomistic modeling of bulk and local structure in liquids and disordered materials by empirical potential structure refinement. Pure Appl. Chem. 80, 1211–1227. doi:10.1351/pac200880061211.

Bras, W., Xu, R., Wicks, J., van der Horst, F., Oversluizen, M., McGreevy, R., van der Lugt, W., 1994. High temperature EXAFS experiments on liquid KPb alloys analysed with the reverse Monte Carlo method. Nucl. Instrum Meth. Phys. Res. A 346, 394–398. doi:10.1016/0168-9002(94)90728-5.

Bunker, G., 1983. Application of the ratio method of EXAFS analysis to disordered systems. Nucl. Instrum. Methods 207, 437–444. doi:10.1016/0167-5087(83)90655-5.

Canche-Tello, J., Vargas, M.C., Hernandez-Cobos, J., Ortega-Blake, I., Leclercq, A., Solari, P.L., Den Auwer, C., Mustre de Leon, J., 2014. Interpretation of X-ray absorption spectra of As(III) in solution using Monte Carlo simulations. J. Phys. Chem. A 118, 10967–10973. doi:10.1021/jp5061232.

Capano, G., Milne, C.J., Chergui, M., Rothlisberger, U., Tavernelli, I., Penfold, T.J., 2015. Probing wavepacket dynamics using ultrafast x-ray spectroscopy. J. Phys. B: Atomic, Molecular and Optical Physics 48, 214001. doi:10.1088/0953-4075/48/21/214001.

Clausen, B.S., Nørskov, J.K., 2000. Asymmetric pair distribution functions in catalysts. Top. Catal. 10, 221–230. doi:10.1023/A:1019196908404.

Dalba, G., Fornasini, P., Grazioli, M., Rocca, F., 1995. Local disorder in crystalline and amorphous germanium. Phys. Rev. B 52, 11034–11043. doi:10.1103/PhysRevB.52.11034.

Dalba, G., Fornasini, P., Rocca, F., 1993. Cumulant analysis of the extended X-ray-absorption fine structure of β-AgI. Phys. Rev. B 47, 8502–8514. doi:10.1103/PhysRevB.47.8502.

D'Angelo, P., Di Nola, A., Filipponi, A., Pavel, N.V., Roccatano, D., 1994. An extended x-ray absorption fine structure study of aqueous solutions by employing molecular dynamics simulations. J. Chem. Phys. 100, 985–994. doi:10.1063/1.466581.

D'Angelo, P., Di Nola, A., Mangoni, M., Pavel, N.V., 1996. An extended x-ray absorption fine structure study by employing molecular dynamics simulations: Bromide ion in methanolic solution. J. Chem. Phys. 104, 1779–1790. doi:10.1063/1.471711.

Di Cicco, A., 1995. EXAFS multiple-scattering data-analysis: GNXAS methodology and applications. Physica B 208-209, 125–128. doi:10.1016/0921-4526(94)00647-E.

Di Cicco, A., Minicucci, M., Principi, E., Witkowska, A., Rybicki, J., Laskowski, R., 2002. Testing interaction models by using x-ray absorption spectroscopy: solid Pb. J. Phys.: Condens. Matter 14, 3365. doi:10.1088/0953-8984/14/12/321.

Di Cicco, A., Trapananti, A., 2005. Reverse Monte Carlo refinement of molecular and condensed systems by X-ray absorption spectroscopy. J. Phys.: Condens. Matter 17, S135–S144. doi:10.1088/0953-8984/17/5/014.

Duan, Z., Li, Y., Timoshenko, J., Chill, S.T., Anderson, R.M., Yancey, D.F., Frenkel, A.I., Crooks, R.M., Henkelman, G., 2016. A combined theoretical and experimental EXAFS study of the structure and dynamics of Au147 nanoparticles. Catal. Sci. Technol. 6, 6879–6885. doi:10.1039/C6CY00559D.

Ershov, N.V., Ageev, A.L., Vasin, V.V., Babanov, Y.A., 1981. A new interpretation of EXAFS spectra in real space: II. A comparison of the regularization technique with the Fourier transformation method. Phys. Status Solidi B 108, 103–111. doi:10.1002/pssb.2221080114.

Filipponi, A., Di Cicco, A., 1995. X-ray-absorption spectroscopy and n-body distribution functions in condensed matter. II. Data analysis and applications. Phys. Rev. B 52, 15135–15149. doi:10.1103/PhysRevB.52.15135.

Filipponi, A., Di Cicco, A., 2000. GNXAS: A software package for advanced EXAFS multiple-scattering calculations and data-analysis. TASK Quarterly 4, 575–669.

Filipponi, A., Di Cicco, A., Natoli, C.R., 1995. X-ray-absorption spectroscopy and n-body distribution functions in condensed matter. I. Theory. Phys. Rev. B 52, 15122–15134. doi:10.1103/PhysRevB.52.15122.

Fornasini, P., Grisenti, R., Dapiaggi, M., Agostini, G., Miyanaga, T., 2017. Nearest-neighbour distribution of distances in crystals from extended X-ray absorption fine structure. J. Chem. Phys. 147, 044503. doi:10.1063/1.4995435.

Gale, J.D., Rohl, A.L., 2003. The general utility lattice program (gulp). Mol. Simul. 29, 291–341.

Gereben, O., Jovari, P., Temleitner, L., Pusztai, L., 2007. A new version of the RMC++ Reverse Monte Carlo programme, aimed at investigating the structure of covalent glasses. J. Optoelectron. Adv. M. 9, 3021–3027.

Gereben, O., Pusztai, L., 2012. RMC_POT: a computer code for reverse Monte Carlo modeling the structure of disordered systems containing molecules of arbitrary complexity. J. Computat. Chem. 33, 2285–2291. doi:10.1002/jcc.23058.

Gurman, S.J., McGreevy, R.L., 1990. Reverse Monte Carlo simulation for the analysis of EXAFS data. J. Phys.: Condens. Matter 2, 9463–9473. doi:10.1088/0953-8984/2/48/001.

Hansen, P.L., Molenbroek, A.M., Ruban, A.V., 1997. Alloy formation and surface segregation in zeolite-supported Pt–Pd bimetallic catalysts. J. Phys. Chem. B 101, 1861–1868. doi:10.1021/jp962771o.

House, S.D., Bonifacio, C.S., Timoshenko, J., Kunal, P., Wan, H., Duan, Z., Li, H., Yang, J.C., Frenkel, A.I., Humphrey, S.M., et al., 2017. Computationally assisted STEM and EXAFS characterization of tunable Rh/Au and Rh/Ag bimetallic nanoparticle catalysts. Microsc. Microanal. 23, 2030–2031.

Jonane, I., Anspoks, A., Kuzmin, A., 2018a. Advanced approach to the local structure reconstruction and theory validation on the example of the W L_3-edge extended X-ray absorption fine structure of tungsten. Modelling Simul. Mater. Sci. Eng. 26, 025004. doi:10.1088/1361-651X/aa9bab.

Jonane, I., Cintins, A., Kalinko, A., Chernikov, R., Kuzmin, A., 2018b. Probing the thermochromic phase transition in $CuMoO_4$ by EXAFS spectroscopy. Phys. Status Solidi B 255, 1800074. doi:10.1002/pssb.201800074.

Jonane, I., Lazdins, K., Timoshenko, J., Kuzmin, A., Purans, J., Vladimirov, P., Gräning, T., Hoffmann, J., 2016. Temperature-dependent EXAFS study of the local structure and lattice dynamics in cubic Y_2O_3. J. Synchrotron Rad. 23, 510–518. doi:10.1107/S1600577516001181.

Kalinko, A., Kuzmin, A., 2011. Static and dynamic structure of $ZnWO_4$ nanoparticles. J. Non-Cryst. Solids 357, 2595–2599. doi:10.1016/j.jnoncrysol.2011.02.027.

Kresse, G., Furthmüller, J., 1996. Efficient iterative schemes for ab initio total-energy calculations using a plane-wave basis set. Phys. Rev. B 54, 11169–11186. doi:10.1103/PhysRevB.54.11169.

Kuzmin, A., Anspoks, A., Kalinko, A., Timoshenko, J., 2016. The use of X-ray absorption spectra for validation of classical force-field models. Z. Phys. Chem. 230, 537–549. doi:10.1515/zpch-2015-0664.

Kuzmin, A., Anspoks, A., Kalinko, A., Timoshenko, J., Kalendarev, R., 2015. External pressure and composition effects on the atomic and electronic structure of $SnWO_4$. Sol. Energy Mater. Sol. Cells 143, 627–634. doi:10.1016/j.solmat.2014.12.003.

Kuzmin, A., Chaboy, J., 2014. EXAFS and XANES analysis of oxides at the nanoscale. IUCrJ 1, 571–589. doi:10.1107/S2052252514021101.

Kuzmin, A., Evarestov, R.A., 2009. Quantum mechanics–molecular dynamics approach to the interpretation of X-ray absorption spectra. J. Phys.: Condens. Matter 21, 055401. doi:10.1088/0953-8984/21/5/055401.

Kuzmin, A., Obst, S., Purans, J., 1997. X-ray absorption spectroscopy and molecular dynamics studies of Zn^{2+} hydration in aqueous solutions. J. Phys.: Condens. Matter 9, 10065–10078. doi:10.1088/0953-8984/9/46/004.

Kuzmin, A., Purans, J., 2000. Dehydration of the molybdenum trioxide hydrates $MoO_3{\cdot}nH_2O$: in situ X-ray absorption spectroscopy study at the Mo K edge. J. Phys.: Condens. Matter 12, 1959–1970. doi:10.1088/0953-8984/12/9/301.

Lapp, A.S., Duan, Z., Marcella, N., Luo, L., Genc, A., Ringnalda, J., Frenkel, A.I., Henkelman, G., Crooks, R.M., 2018. Experimental and theoretical structural investigation of AuPt nanoparticles synthesized using a direct electrochemical method. J. Am. Chem. Soc. 140, 6249–6259. doi:10.1021/jacs.7b12306.

Lee, B.J., Baskes, M., Kim, H., Koo Cho, Y., 2001. Second nearest-neighbor modified embedded atom method potentials for bcc transition metals. Phys. Rev. B 64, 184102. doi:10.1103/PhysRevB.64.184102.

Lee, P.A., Citrin, P.H., Eisenberger, P., Kincaid, B.M., 1981. Extended X-ray absorption fine structure – its strengths and limitations as a structural tool. Rev. Mod. Phys. 53, 769–806. doi:10.1103/RevModPhys.53.769.

Lee, P.A., Pendry, J.B., 1975. Theory of the extended X-ray absorption fine structure. Phys. Rev. B 11, 2795–2811. doi:10.1103/PhysRevB.11.2795.

Leetmaa, M., Wikfeldt, K.T., Pettersson, L.G.M., 2010. SpecSwap-RMC: a novel reverse Monte Carlo approach using a discrete set of local configurations and pre-computed properties. J. Phys.: Condens. Matter 22, 135001. doi:10.1088/0953-8984/22/13/135001.

Lemke, H.T., Kjær, K.S., Hartsock, R., van Driel, T.B., Chollet, M., Glownia, J.M., Song, S., Zhu, D., Pace, E., Matar, S.F., Nielsen, M.M., Benfatto, M., Gaffney, K.J., Collet, E., Cammarata, M., 2017. Coherent structural trapping through wave packet dispersion during photoinduced spin state switching. Nature 8, 15342. doi:10.1038/ncomms15342.

Marx, D., Parrinello, M., 1996. Ab initio path integral molecular dynamics: Basic ideas. J. Chem. Phys. 104, 4077. doi:10.1063/1.471221.

McGreevy, R.L., 2001. Reverse Monte Carlo modelling. J. Phys.: Condens. Matter 13, R877–R913. doi:10.1088/0953-8984/13/46/201.

McGreevy, R.L., Pusztai, L., 1988. Reverse Monte Carlo simulation: A new technique for the determination of disordered structures. Mol. Simul. 1, 359–367. doi:10.1080/08927028808080958.

Metropolis, N., Rosenbluth, A.W., Rosenbluth, M.N., Teller, A.H., Teller, E., 1953. Equation of state calculations by fast computing machines. J. Chem. Phys. 21, 1087–1092. doi:10.1063/1.1699114.

Mino, L., Borfecchia, E., Segura-Ruiz, J., Giannini, C., Martinez-Criado, G., Lamberti, C., 2018. Materials characterization by synchrotron x-ray microprobes and nanoprobes. Rev. Mod. Phys. 90, 025007. doi:10.1103/RevModPhys.90.025007.

Natoli, C.R., Benfatto, M., Della Longa, S., Hatada, K., 2003. X-ray absorption spectroscopy: state-of-the-art analysis. J. Synchrotron Rad. 10, 26–42. doi:10.1107/S0909049502017247.

Okamoto, Y., Akabori, M., Motohashi, H., Itoh, A., Ogawa, T., 2002. High-temperature XAFS measurement of molten salt systems. Nucl. Instrum. Meth. Phys. Res. A 487, 605–611. doi:10.1016/S0168-9002(01)02202-1.

Palmer, B.J., Pfund, D.M., Fulton, J.L., 1996. Direct modeling of exafs spectra from molecular dynamics simulations. J. Chem. Phys. 100, 13393–13398. doi:10.1021/jp960160q.

Plimpton, S., 1995. Fast parallel algorithms for short-range molecular dynamics. J. Comp. Phys. 117, 1–19. doi:10.1006/jcph.1995.1039.

Rehr, J.J., Albers, R.C., 2000. Theoretical approaches to X-ray absorption fine structure. Rev. Mod. Phys. 72, 621–654. doi:10.1103/RevModPhys.72.621.

Rehr, J.J., Kas, J.J., Prange, M.P., Sorini, A.P., Takimoto, Y., Vila, F., 2009. Ab initio theory and calculations of X-ray spectra. C. R. Phys. 10, 548–559. doi:10.1016/j.crhy.2008.08.004.

Rehr, J.J., Kas, J.J., Vila, F.D., Prange, M.P., Jorissen, K., 2010. Parameter-free calculations of X-ray spectra with FEFF9. Phys. Chem. Chem. Phys. 12, 5503–5513. doi:10.1039/B926434E.

Ruiz-Lopez, M., Loos, M., Goulon, J., Benfatto, M., Natoli, C., 1988. Reinvestigation of the EXAFS and XANES spectra of ferrocene and nickelocene in the framework of the multiple scattering theory. Chem. Phys. 121, 419–437. doi:10.1016/0301-0104(88)87246-X.

Sayers, D.E., Stern, E.A., Lytle, F.W., 1971. New technique for investigating noncrystalline structures: Fourier analysis of the extended X-ray–absorption fine structure. Phys. Rev. Lett. 27, 1204–1207. doi:10.1103/PhysRevLett.27.1204.

Sevillano, E., Meuth, H., Rehr, J.J., 1979. Extended X-ray absorption fine structure Debye-Waller factors. I. Monatomic crystals. Phys. Rev. B 20, 4908–4911. doi:10.1103/PhysRevB.20.4908.

Soler, J.M., Artacho, E., Gale, J.D., Garcia, A., Junquera, J., Ordejon, P., Sanchez-Portal, D., 2002. The SIESTA method for ab initio order-N materials simulation. J. Phys: Condens. Matter 14, 2745. doi:10.1088/0953-8984/14/11/302.

Stern, E.A., Sayers, D.E., Lytle, F.W., 1975. Extended x-ray-absorption fine-structure technique. III. Determination of physical parameters. Phys. Rev. B 11, 4836–4846. doi:10.1103/PhysRevB.11.4836.

Sun, X., Sun, F., Sun, Z., Chen, J., Du, X., Wang, J., Jiang, Z., Huang, Y., 2017. Disorder effects on EXAFS modeling for catalysts working at elevated temperatures. Rad. Phys. Chem. 137, 93–98. doi:10.1016/j.radphyschem.2016.01.039.

Timoshenko, J., Anspoks, A., Cintins, A., Kuzmin, A., Purans, J., Frenkel, A.I., 2018. Neural network approach for characterizing structural transformations by X-ray absorption fine structure spectroscopy. Phys. Rev. Lett. 120, 225502. doi:10.1103/PhysRevLett.120.225502.

Timoshenko, J., Anspoks, A., Kalinko, A., Kuzmin, A., 2014a. Analysis of extended X-ray absorption fine structure data from copper tungstate by the reverse Monte Carlo method. Phys. Scr. 89, 044006. doi:10.1088/0031-8949/89/04/044006.

Timoshenko, J., Anspoks, A., Kalinko, A., Kuzmin, A., 2017. Thermal disorder and correlation effects in anti-perovskite-type copper nitride. Acta Mater. 129, 61–71. doi:10.1016/j.actamat.2017.02.074.

Timoshenko, J., Kuzmin, A., 2009. Wavelet data analysis of EXAFS spectra. Comput. Phys. Commun. 180, 920–925. doi:10.1016/j.cpc.2008.12.020.

Timoshenko, J., Kuzmin, A., Purans, J., 2012. Reverse Monte Carlo modeling of thermal disorder in crystalline materials from EXAFS spectra. Comput. Phys. Commun. 183, 1237–1245. doi:10.1016/j.cpc.2012.02.002.

Timoshenko, J., Kuzmin, A., Purans, J., 2014b. EXAFS study of hydrogen intercalation into ReO_3 using the evolutionary algorithm. J. Phys.: Condens. Matter 26, 055401. doi:10.1088/0953-8984/26/5/055401.

Todorov, I.T., Smith, W., Trachenko, K., Dove, M.T., 2006. DL_POLY_3: new dimensions in molecular dynamics simulations via massive parallelism. J. Mat. Chem. 16, 1911–1918. doi:10.1039/B517931A.

Tranquada, J.M., Ingalls, R., 1983. Extended x-ray–absorption fine-structure study of anharmonicity in CuBr. Phys. Rev. B 28, 3520–3528. doi:10.1103/PhysRevB.28.3520.

Tucker, M.G., Keen, D.A., Dove, M.T., Goodwin, A.L., Hui, Q., 2007. RMCProfile: reverse Monte Carlo for polycrystalline materials. J. Phys.: Condens. Matter 19, 335218. doi:10.1088/0953-8984/19/33/335218.

Vaccari, M., Fornasini, P., 2006. Einstein and Debye models for EXAFS parallel and perpendicular mean-square relative displacements. J. Synchrotron Radiat. 13, 321–325. doi:10.1107/S0909049506018504.

van Oversteeg, C.H.M., Doan, H.Q., de Groot, F.M.F., Cuk, T., 2017. In situ X-ray absorption spectroscopy of transition metal based water oxidation catalysts. Chem. Soc. Rev. 46, 102–125. doi:10.1039/C6CS00230G.

VandeVondele, J., Krack, M., Mohamed, F., Parrinello, M., Chassaing, T., Hutter, J., 2005. Quickstep: Fast and accurate density functional calculations using a mixed Gaussian and plane waves approach. Comp. Phys. Commun. 167, 103–128. doi:10.1016/j.cpc.2004.12.014.

Vila, F.D., Rehr, J.J., Rossner, H.H., Krappe, H.J., 2007. Theoretical X-ray absorption Debye-Waller factors. Phys. Rev. B 76, 014301. doi:10.1103/PhysRevB.76.014301.

Wicks, J.D., Borjesson, L., Bushnell-Wye, G., Howells, W.S., McGreevy, R.L., 1995. Modelling the structure and ionic conduction of $(AgI)_x(AgPO_3)_{1-x}$ glasses. Phys. Scr. T57, 127–132. doi:10.1088/0031-8949/1995/T57/022.

Yang, Y., Kawazoe, Y., 2012. Characterization of zero-point vibration in one-component crystals. EPL 98, 66007. doi:10.1209/0295-5075/98/66007.

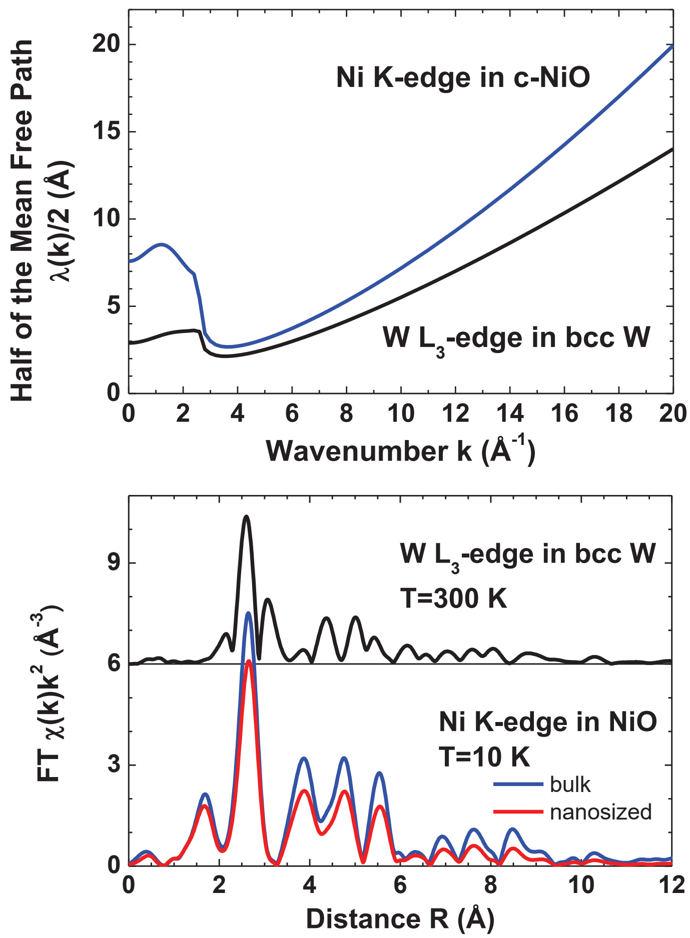

Figure 1: Upper panel: Calculated photoelectron mean free path (MFP) $\lambda(k)$ for c-NiO and bcc W. Lower panel: Fourier transforms of the experimental W L_3-edge and Ni K-edge EXAFS spectra $\chi(k)k^2$ in bulk and nanosized NiO at $T = 10$ K and in bcc tungsten at $T = 300$ K, respectively.

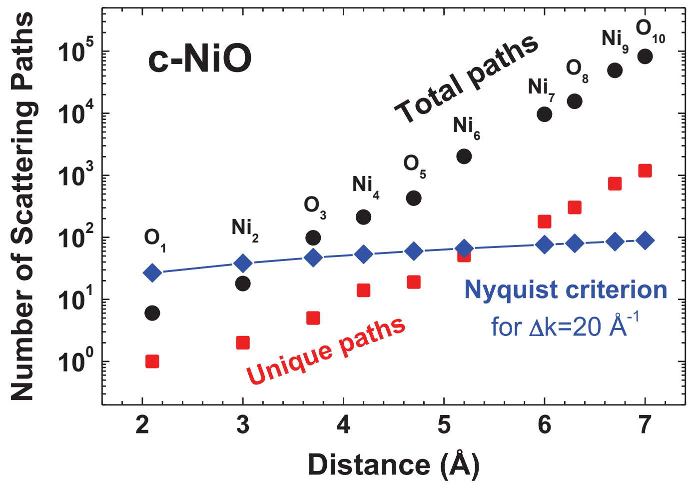

Figure 2: The dependence of the number of scattering paths on the cluster size around the absorbing nickel atom in NiO.

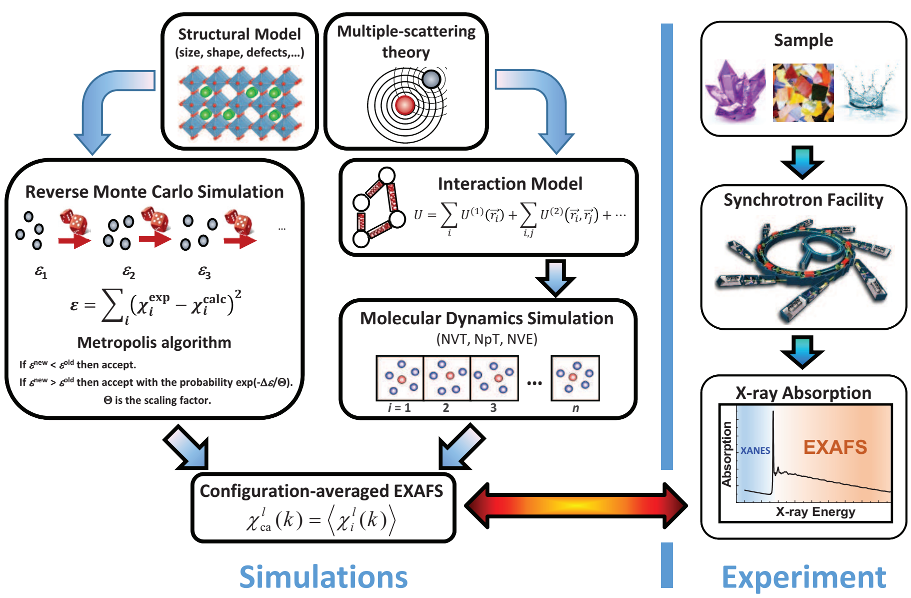

Figure 3: Scheme of EXAFS analysis using reverse Monte Carlo and molecular dynamics methods.

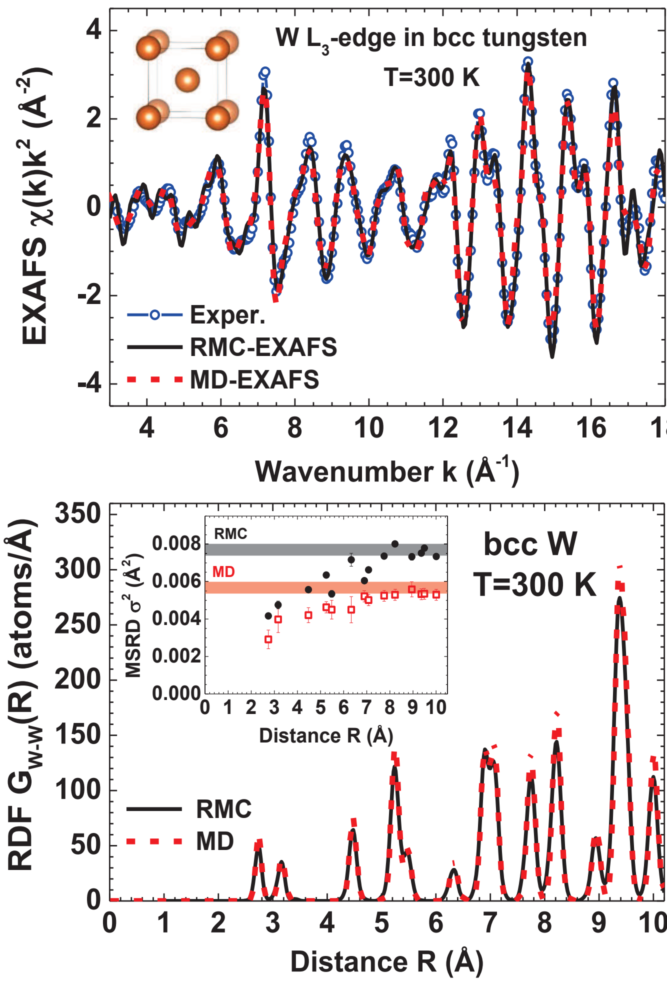

Figure 4: Upper panel: Comparison of the experimental and calculated by the RMC and MD methods W L_3-edge EXAFS $\chi(k)k^2$ of bcc W at $T = 300$ K. Lower panel: Radial distribution functions (RDF) $G_{W-W}(R)$ obtained by RMC and MD simulations. Inset: Dependence of the MSRD $\sigma^2_{W-W}(R)$ on distance. Two horizontal lines correspond to a sum of two MSDs of tungsten.

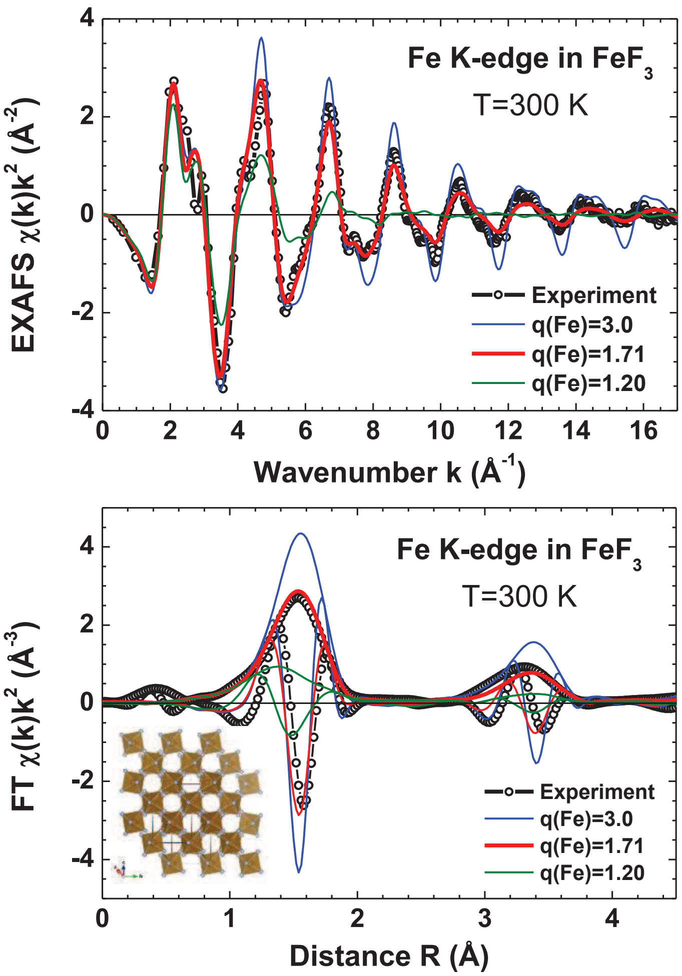

Figure 5: Comparison of the experimental and calculated Fe K-edge MD-EXAFS $\chi(k)k^2$ spectra and their Fourier transforms (FTs) (modulus and imaginary parts are shown) in FeF_3 at T=300 K. Only few spectra calculated for different effective iron charges are shown for clarity.

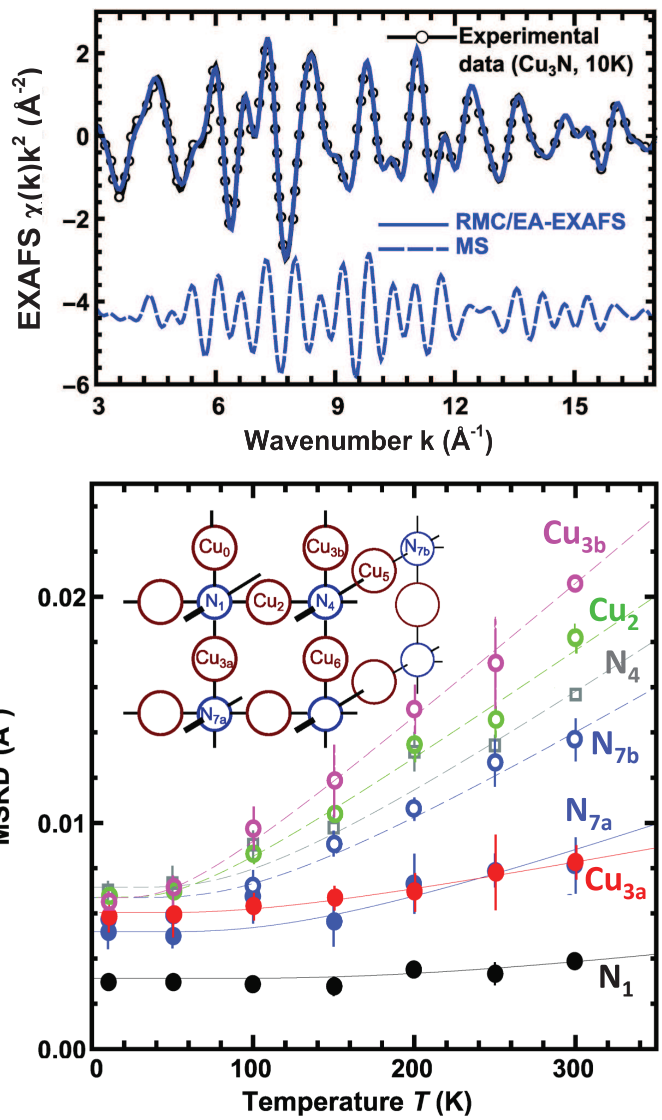

Figure 6: Upper panel: Comparison of the experimental and calculated CA Cu K-edge EXAFS spectra of Cu_3N at T=10 K. Dashed line shows the total MS contribution. Lower panel: Temperature dependencies of the MSRD factors for selected Cu–N and Cu–Cu atom pairs in Cu_3N. Inset: The fragment of the Cu_3N structure. Coordination shells around the absorber Cu_0 are labelled.

Institute of Solid State Physics, University of Latvia as the Center of Excellence has received funding from the European Union's Horizon 2020 Framework Programme H2020-WIDESPREAD-01-2016-2017-TeamingPhase2 under grant agreement No. 739508, project CAMART²